Teknik Dergi, 2022 12283-12308, Paper 682

An Investigation on Force Modification Factors in Cold-Formed Steel Structures

Macit YURTSEVER[1]
Serdar SOYÖZ[2]

ABSTRACT

The Force Modification Factors defined in the Turkish Seismic Code (2018) for cold-formed steel structures are examined within the scope of this paper. Experimental and analytical studies are carried out on a real-life structure to investigate if the defined coefficients are practically applicable. An Ambient Vibration Survey is implemented to obtain the characteristic modal periods of the building, which is then modelled in computing environment through modal calibration. Additional laboratory experiments are carried out to determine a mathematical relationship for the connections between the bracing and the frame members of the building. Performance analysis is conducted to analyze the nonlinear behavior of the structure, and the force modification factors are evaluated. It is observed that the computed values from the analyses are generally within the range of what is defined in the Code, if not greater. Several suggestions as to where the Code content could be improvised are also included.

Keywords: Cold-formed steel, performance analysis, force modification factors, real-life building, Turkish Seismic Code 2018.

1. INTRODUCTION

Construction industry has only become familiar with cold-formed steel (CFS) structures for a couple of decades, but thanks to technological improvements and development of sophisticated testing facilities, there are already plenty of available data (codes, recommendations and other written sources) to be used in the design of such structures. There are already numerous projects in Turkey, as well where cold-formed steel is utilized. Considering that Turkey frequently falls prone to earthquakes with mild to severe intensities, this growing construction sector has recently seen an increasing interest, and the newest Turkish Seismic Code (TSC 2018) (1) provides some very helpful and elaborate design

Note:
- This paper has been received on August 4, 2021 and accepted for publication by the Editorial Board on February 18, 2022.
- Discussions on this paper will be accepted by September 30, 2022.

• https://doi.org/10.18400/tekderg.977677

1 Sur Yapi A.S., Istanbul, Turkey
macityurtsever@gmail.com - https://orcid.org/0000-0002-3402-3847

2 Department of Civil Engineering, Boğaziçi University, Istanbul, Turkey
serdar.soyoz@boun.edu.tr - https://orcid.org/0000-0002-5502-6545

methodologies on CFS structures. Yet some of the aspects that have entered the Code still require more research to be finalized, and force modification factors are among those aspects. This paper will specifically focus on the ductility-related modification factor (described as the Structural Behavior Factor in the Code), which are defined as R=4 for structural systems with high ductility, and R=3 for structural systems with limited ductility.

Plenty of valuable reference is available covering both experimental and analytical research previously done by academics and other professionals. Della Corte *et al.* (2) provided and discussed the results of a numerical study on seismic deformation demand to sheathed CFS structures. It is part of a wider research, also involving calibration of the numerical model against data from physical tests, which were conducted by Landolfo *et al.* (3) through an extensive experimental study on the seismic behavior of cold-formed steel stud shear walls. Dubina (4) provided an extensive examination that summarizes the results and findings of monotonic and cyclic tests performed on full-scale shear panels, tests on various connection details, and in-situ ambient vibration tests on a house under construction. Velchev *et al.* (5) evaluated typical strap braced wall configurations with respect to their strength and inelastic behavior. Nithyadharan and Kalyanaraman (6) presented the results of an experimental study on the behavior and strength of the CFS shear wall panel, when subjected to monotonically increasing and reversed cyclic in-plane shear deformation. Their paper also proposes a 'simplified method' for evaluating the shear strength of the wall panel as governed by the sheathing-to-frame screw connections' strength. Shamim and Rogers (7) described the numerical modelling using OpenSees for shear walls constructed of cold-formed steel framing and flat steel sheathing. The paper also includes an analytical example of a two-story office building modelled in OpenSees. Sato and Uang (8) verified the adequacy of the proposed seismic performance factors for the newly developed Cold-Formed Steel Special Bolted Moment Frames in the AISI S110 Seismic Standard using the FEMA P695 methodology. Within the scope of an Italian research project called RELUIS-DPC 2010-2013, undertaken at the University of Naples, Iuorio *et al.* (9) investigated the seismic behavior of strap-braced stud walls. Bian *et al.* (10) combined two types of analytical modelling techniques to provide a highly versatile shear wall model capable of capturing both fastener-based and member-based limit states in the shear wall. Senkardesler *et al.* (11) presented the results of dynamic and cyclic experiments conducted on two different 3-D and 2-storey models, which were two CFS structures with and without infill materials. Borzoo *et al.* (12) investigated the stiffness, strength and failure modes of CFS shear panels under monotonic loading, using ABAQUS software. Madsen *et al.* (13) provided guidelines for NEHRP Seismic Design Technical Brief No.12, which is an extensive document specialized for cold-formed steel structures, including basic construction outlines as well as seismic design guidelines and experimental literature. Karabulut (14) performed cyclic tests on a number of specimens using various configurations in order to observe the effects of board type, steel thickness, screw spacing and axial loads on structural performance of CFS shear panels. Leng *et al.* (15) performed shake table tests on a two-story CFS-framed building with OSB sheathed shear walls. FE models of the building during its various test phases were also developed in OpenSees. Riahi *et al.* (16) evaluated the seismic performance factor of CFS frames with K-shaped bracings in accordance with Iranian seismic code, again by utilizing the OpenSees software. Most recently, Haghpanah and Schafer (17) provided fragility functions for various configurations of CFS-framed shear walls, after investigating as to which displacement levels they could be subjected before a probability of failure occurs.

The motivation of this study is to investigate if the force modification factors defined in TSC 2018 for cold-formed steel structures are reliable. In this regard, it may be fair to assume it mostly differs from the aforementioned literature. However, there are minor links to the work of Karabulut (14), and it overlap with the work of Riahi *et al*. (16). At this point, it must be said that it does not aim to fully challenge the specifications provided in TSC 2018. The sole intent is to get an insight on how the computational values fare against the Code recommendations, and to provide a starting point for further studies of similar focus. Although this study only considers the factors given in TSC 2018, the subjects covered within may as well be interpreted and made available for use with other codes and specifications.

In order to have a reliable basis for verification of the factors, an ambient vibration survey is performed on a real-life CFS structure, and a faithful representation of the structure is generated through an analytical model. Then the model is used for performance assessment and other required computations related to the objective. Also, cyclic tests are performed on typical specimens to calibrate various structural parameters.

2. AMBIENT VIBRATION TEST ON A REAL-LIFE STRUCTURE

2.1. General Information

A two-story CFS building was provided by courtesy of Akkon Celik Yapi Sistemleri A.S., builders of the building, and has been monitored through ambient vibration tests. The equipment used in this test is manufactured by Kinemetrics, which is essentially a 12-channel substation with a sampling rate of 200 Hz and is provided by the Structures Laboratory of Boğaziçi University.

Figure 1 - Some images of the typical mirror-villa used for AVT

The building is situated in one of the resorts close to the Enez Harbour in Trapez district of Enez (Edirne). This resort consists of monotype two-story mirror-villas and is one of many similarly constructed groups of villas that can be observed around in the district. The building considered in this study was presumably built in the early 2000s, and is understandably not compliant with the TSC 2018. It has approximately a 12.0 m by 6.7 m footprint (see Figure 1). Sensors of the monitoring device were all installed on the second floor (slab or ceiling) in the left-half of the building since the other half was not available for testing purposes because of its residents at the time.

For this test, a total of 10 sensors were installed. The only sensors that were placed on the wall close to the ceiling are #9 and #10, and the rest of the sensors were all placed on the second story floor, as demonstrated in Figures 2(a)-(b). More detailed information regarding the ambient vibration test and the subsequent results is provided by Yurtsever (18), only the Power Spectral Density (PSD) is covered here for the sake of simplicity.

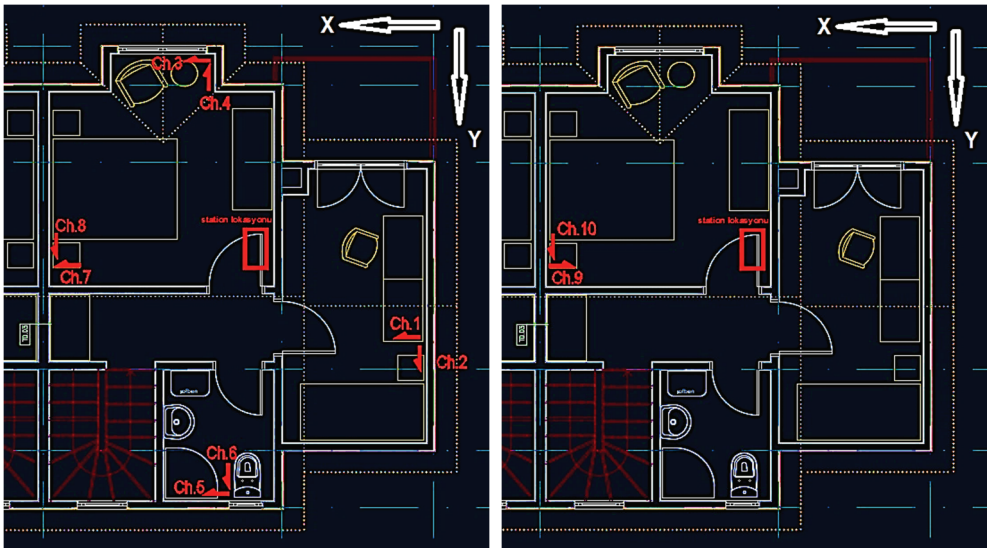

(a) Upper floor slab *(b) Upper floor ceiling*

Figure 2 - Sensor layouts on the upper floor of the test building

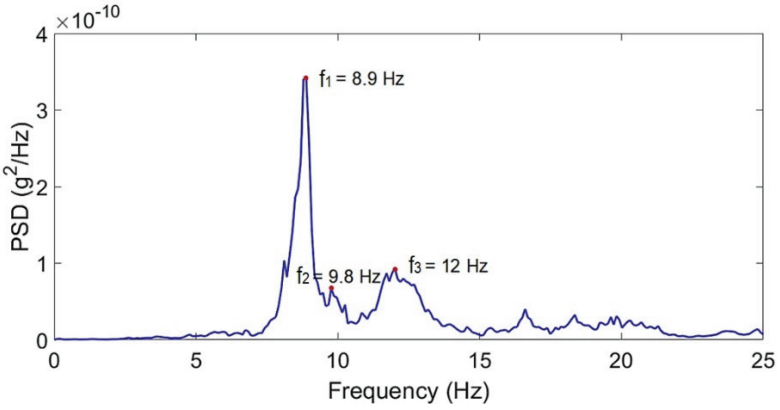

Figure 3 - Windowed and filtered results of the Fast Fourier Transformation

Power Spectral Density was obtained by 'windowing' the total length data, for which the length was assumed as 2048 data-points. The sampling rate of the data was 200 Hz, the same

as obtained from the test. Cut-off frequency of 50 Hz and an overlap (averaging rate) of 50% was used in the analysis. Also, a high-pass filter (0.15~0.50 Hz) was applied to all acceleration records.

As can be traced from Figure 3, the first natural frequency of the building appears to be 8.9 Hz (T_1 = 0.112 sec) in X-direction (along the longer dimension of the building), and the second natural frequency is 9.8 Hz (T_2 = 0.102 sec) in Y-direction (along the shorter dimension). The third natural frequency is about 12 Hz ($T_3 \approx 0.08$ sec).

2.2. Finite Element Modelling

In order to carry on with the performance assessment phase, a 3-dimensional analysis model was prepared using the software SAP2000 (19) in line with the information provided by Akkon Celik Yapi Sistemleri A.S. The walls of the structure incorporate double layers of OSB panels, with a thickness of 12.5 mm each. The dimensions of the panels are 1220 mm (width) by 2440 mm (height), with a stud spacing of 610 mm on average. The screw distance is reported to be 150 mm on the exterior studs (of each panel) and 300 mm on the interior studs. The same panel and screw configuration is also used for the slabs. All panels and slabs are modelled as 4-node shell elements, rigorously meshed at appropriate sizes. It was observed that floor diaphragms caused numerical difficulties and unrealistic/unreliable FE behavior during the analyses. Thus, the floor members of the building (i.e. slabs and beams alike) were explicitly modelled and no diaphragms were assigned at floor levels.

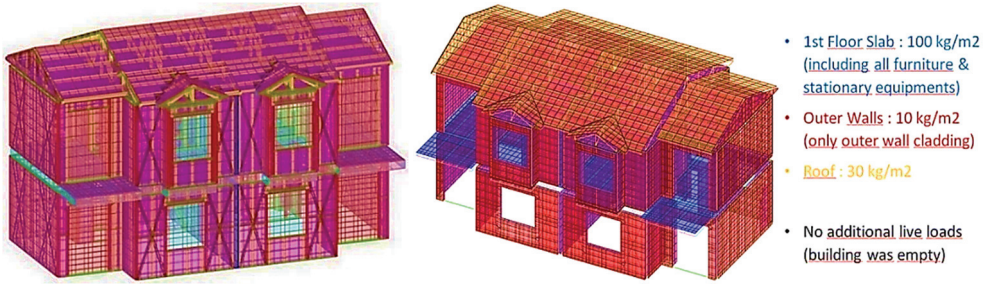

(a) 3D model *(b) Applied loads*

Figure 4 - Graphical representation of the analytical model

Apart from the project drawings, the mechanical properties of the panels and screws are defined similar to those provided by Karabulut (14). Suspended ceiling is not included in the model, and minor dimensional differences between the real-life structure and the analytical model, especially around the staircase, are ignored. The entire FE model of the building rests on simple supports, located at each frame intersection at the base level. Considering that the site was mostly uninhabited at the time of the visit, and that the present layout of the household consisted of limited furniture, a cautious approach was adopted for load definitions. Figures 4(a)-(b) illustrate the 3-D analysis model, along with the external loads applied on the structure.

The calibration of the analytical model is done through modal analysis. More detailed information about the modal calibration is provided by Yurtsever (18), and the modal results are obtained as given in Table 1. As the analyses progressed, there occurred a necessity to improve the analytical model, since the obtained results were far from being satisfactory (i.e. low modal participating mass ratios). Modifications yielded more stable results, as demonstrated in the table. Improvements to the model include updating the stiffness of the link elements, and the introduction of some rigid elements in order to counter unrealistic FE behavior, which are thoroughly explained by Yurtsever (20).

Table 1 - Structural modal periods after updated link properties

Comparison of Natural Vibration Modes	1st Natural Vibration Mode	Dir.	Modal Participating Mass Ratio	2nd Natural Vibration Mode	Dir.	Modal Participating Mass Ratio	3rd Natural Vibration Mode	Dir.	Modal Participating Mass Ratio
Experimental Results	0.115 sec.	X	N.A.	0.107 sec.	Y	N.A.	0.080 sec.	X / Y	N.A.
Analytical Results									
W/O Links - Rigid Connections	0.072 sec.	X	44%	0.060 sec.	Y	66.6%	0.043 sec.	X	20%
W/ Links (Elastic Stiffness) No Doors & Windows	0.130 sec.	X	37.7%	0.117 sec.	Y	32.3%	0.079 sec.	Y	27.5%
W/ Links (Elastic Stiffness) External Doors & Windows	0.116 sec.	X	36.5%	0.115 sec.	Y	39.9%	0.074 sec.	Y	19.2%
W/ Links (Updated Stiffness) External Doors & Windows	0.121 sec.	X	75.2%	0.114 sec.	Y	82.7%	0.094 sec.	X	8.7%

2.3. Additional Improvements to the FE Model

In order to verify and improve the link properties of the brace-to-frame connections used in the analytical model, two additional experiments were carried out in the Structures Laboratory of Boğaziçi University. The test specimens were prepared by combining two 1200x2400 mm CFS frames and assembling 70x1.5 mm strips as braces on both sides. Figures 5(a)-(b) illustrate both the general dimensions, and the sensor and/or strain gauge layout of the specimens, whereas Figures 6(a)-(b) provide the relevant analytical model details.

The first specimen was equipped with 11 mm gypsum, and the second was equipped with 11 mm OSB panels on both sides. Screw spacing on both specimens is 150 mm on the outer studs and girders, including the middle stud. The spacing on the interior studs and girders is 300 mm. From the three loading protocols proposed by ASTM E2126-11 (21), Test Method C (CUREE Basic Loading Protocol) was applied, using a push-pull type actuator with a maximum stroke of 200 mm. The resultant force-displacement curves for each specimen are given in Figures 7(a)-(b), respectively.

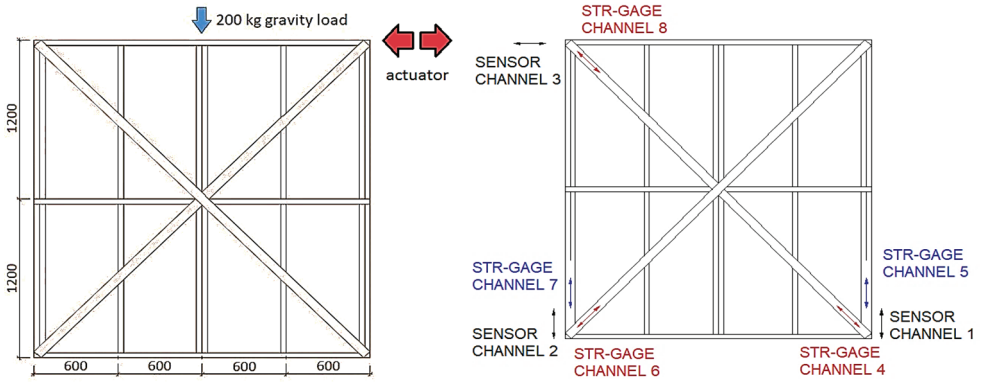

(a) Overall dimensions *(b) Sensor / strain gauge orientations*

Figure 5 - General layout of the test specimens

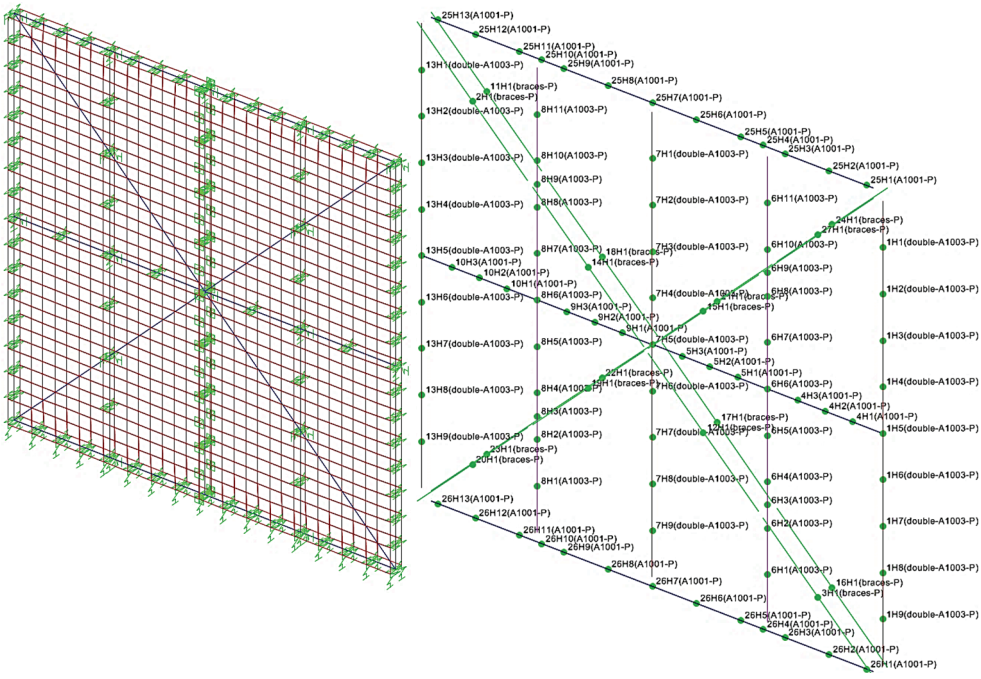

(a) Link element assignments *(b) Plastic hinge assignments*

Figure 6 - A detailed representation of the analysis model

As stated previously, these experiments are aimed at generating a reliable force-displacement relationship for the brace-to-frame connections. Using two different panel types within the specimens helps to verify that the proposed relationship works for both panel types. An updated link property is defined (see Figure 8) and is verified in accordance with the test results. Additional nonlinearity is considered in the analysis in the form of plastic hinges in the studs, girders and braces, which are extensively covered in the following chapter.

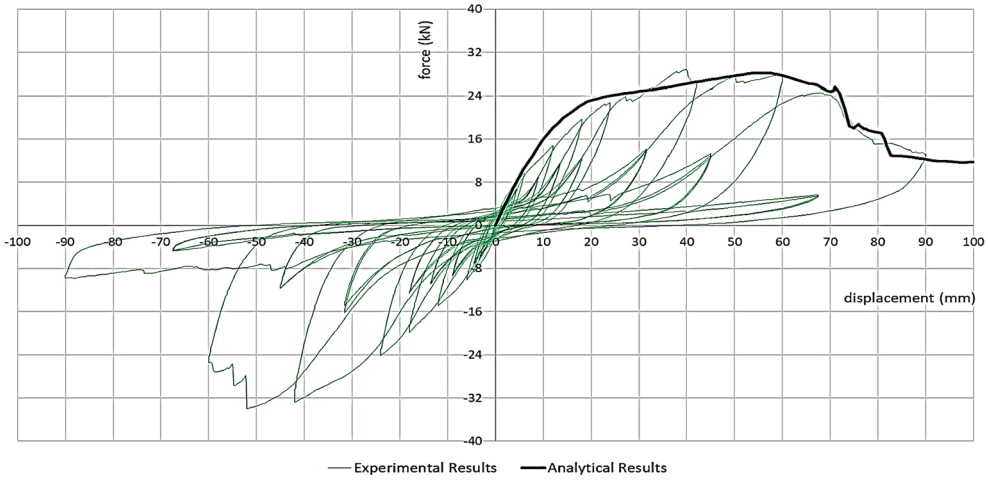

(a) Actuator force vs. panel top displacement for CFS frame with gypsum panels

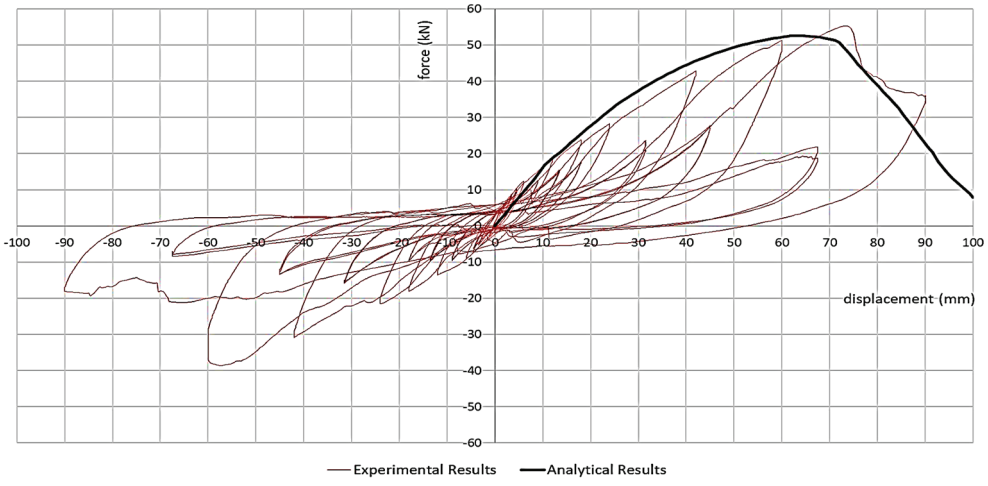

(b) Actuator force vs. panel top displacement for CFS frame with OSB panels

Figure 7 - Cyclic test results of the braced CFS frames, superimposed with analysis results

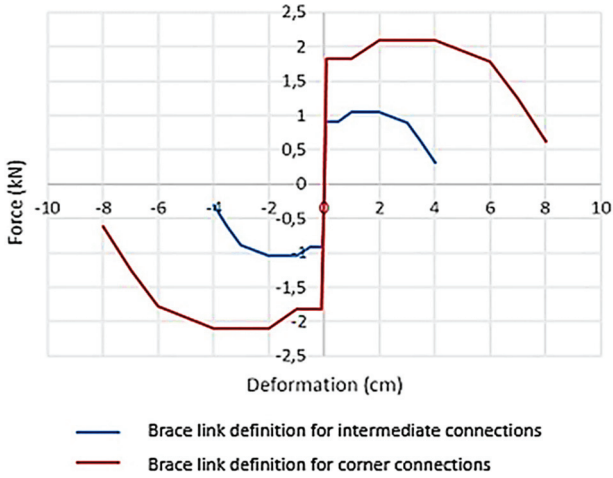

Figure 8 - The proposed force-deformation curves for the brace connections

3. PERFORMANCE ASSESSMENT OF THE FINALIZED FE MODEL

3.1. Performance-Based Analyses: Introduction

In line with the assumptions and revisions made during experimental analyses, all braces in the analytical model of the Enez building have been redefined as two separate frame elements, connected to the CFS frame via additional two-joint links. Force-displacement behavior of the said links has been demonstrated in Figure 8. Table 2 displays the structural modes of the analytical model after these final improvements.

Table 2 - modal periods after updating the link properties of the brace connections

Comparison of Natural Vibration Modes	1st Natural Vibration Mode	Dir.	Modal Participating Mass Ratio	2nd Natural Vibration Mode	Dir.	Modal Participating Mass Ratio	3rd Natural Vibration Mode	Dir.	Modal Participating Mass Ratio
Experimental Results	0.115 sec.	X	N.A.	0.107 sec.	Y	N.A.	0.080 sec.	X / Y	N.A.
Analytical Results									
W/ Links (Updated Stiffness) External Doors & Windows	0.121 sec.	X	75.2%	0.114 sec.	Y	82.7%	0.094 sec.	X	8.7%
W/ Links (Updated Brace Links) No Doors &Windows	0.120 sec.	Y	43%	0.117 sec.	X	54.1%	0.099 sec.	Y	32.9%

Regarding the pushover analyses, hinge definitions and assignments have also been modified. In studs for example, deformation controlled axial hinges are assigned along every one-tenth of the stud length. Similarly for girders around the door and window openings, deformation controlled axial hinges are defined along every one-fifth, one-fourth, one-third or half length

of the girder (depending on the girder length). Hinge interval is selected so that a sufficient level of nonlinearity is covered through a single frame element. After thoroughly examining the initial (pushover) analysis results and observing that some of the upper girders of the first-floor walls experience high compressive forces at the later stages of the analysis, it is acknowledged that these members, too, sustain significant nonlinear deformations. Thus, additional hinge definitions are made for girders at story levels in a similar manner. Formation of any shear-induced plastic hinges are ignored since there is no evident and reliable data in recent literature regarding this concept. For braces, deformation controlled axial hinges are considered and assigned at the mid-span of the braces, for which a small compression limit is defined to account for buckling. Hinges in all elements at rooftop level are also ignored.

A sample definition for stud hinges is given in Figure 9. As can be noticed, the value of applicable compressive stress immediately drops to 5% of the assumed buckling stress level, just after the yield strain is attained (point C [yellow dots] and point D [orange dots]). A typical stress-strain relationship is utilized to define controlling parameters, in order to keep the calculations as simple as possible. Hinge length is taken as approximately the half-depth of the section. Positive stress limit is taken as the yield stress, and the corresponding strain limit is obtained by simply dividing the yield stress by the modulus of elasticity (of steel). Negative stress and strain limits are calculated using the software GBTUL (22), CUFSM (23) and CUTWP (24), which have been specifically designed for evaluating the buckling modes of CFS sections. Their respective results are compared, and the lowest value is assigned as the buckling load of the member and divided by the cross-section area to obtain the relevant stress values.

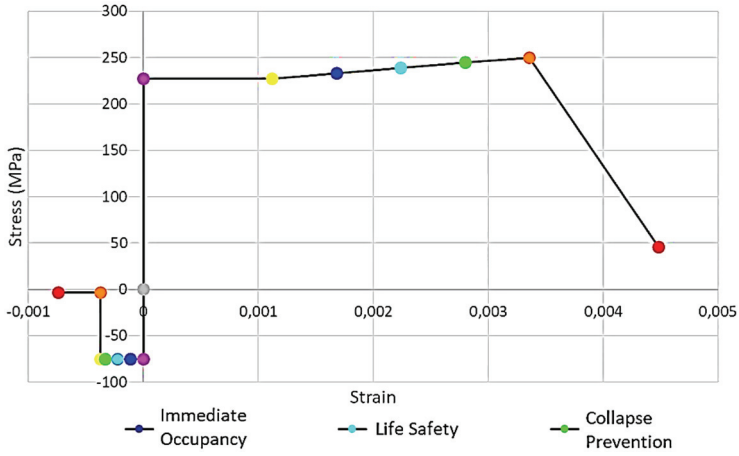

Figure 9 - Typical hinge definition (example given for studs)

For buckling mode calculations, braces are assumed to be clamped at both ends, considering that adjacent portions of the brace would both have to buckle towards the inside of a shear wall, and the rotations where they are fixed to the frame would then be practically zero. Studs are assumed to be free at one end and clamped at the other. Also, only half-length of the

member is considered since it was observed during laboratory tests that specimens showed no deformations around the mid-height of the studs (hence the clamped-end assumption). Girders are again assumed to be free at one end and clamped at the other. Member length is taken as the unrestrained distance between each stud (600 mm).

Post-buckling response of the elements (if there could be any) is neglected since their reliability is not verified for this specific model and/or requires extensive and time-consuming research. Instead, plastic hinges in compressive members are defined such that their load carrying capacity is diminished as soon as the buckling load limit is reached. A detailed interpretation for the post-buckling option is provided in Chapter 3.3, and it was eventually concluded that post-buckling need not be taken into consideration.

3.2. Performance-Based Analyses: Results

The resultant pushover curves are illustrated in Figures 10(a)-(b). There is a notable kink at the beginning of each curve, corresponding to the majority of the braces buckling at the initial stages of the analysis, which will be covered in detail in the following sections. It is also worth mentioning that pushover curves are only plotted up to the point where the analysis results are found to be reliable.

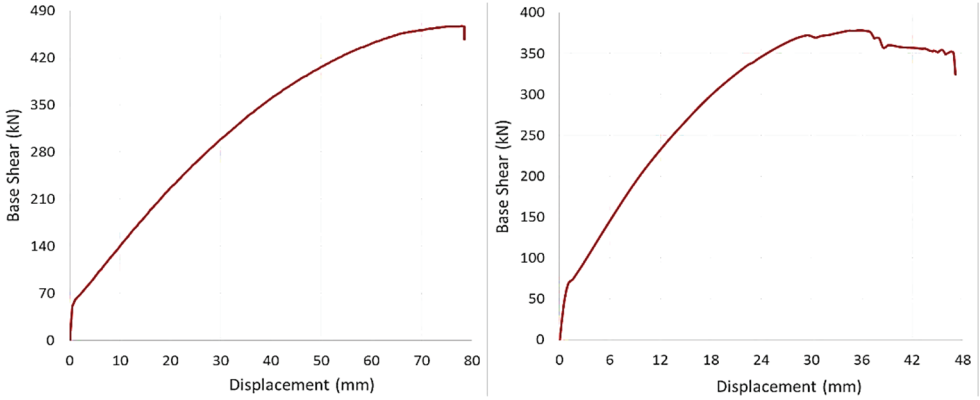

(a) X-direction *(b) Y-direction*

Figure 10 - The resultant pushover curves

A general representation for the resultant deformed shapes of the building after the pushover analyses in X-direction and Y-direction are given in Figures 11(a)-(b), respectively. Note the damage concentration in the structural elements around the stairs and back doors. There is also a slight damage propagation around the first-floor windows. Also, some damage appears to be concentrated in the structural elements on the central walls and around the first-floor windows, especially for the pushover analysis in Y-direction.

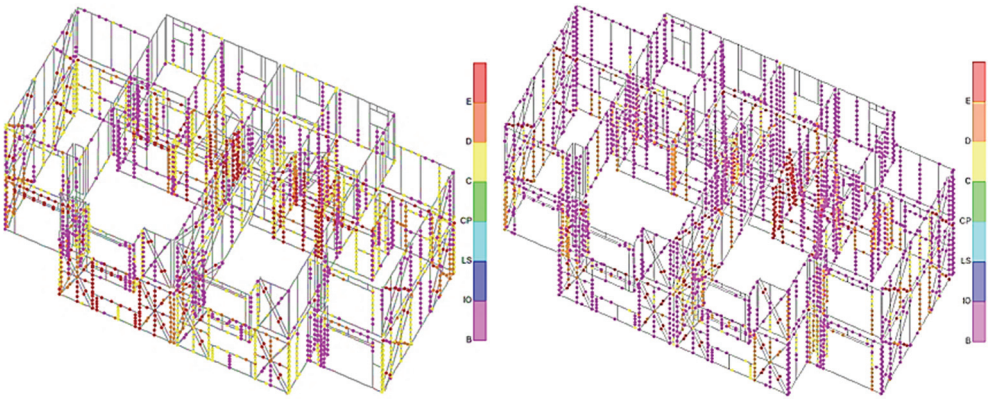

(a) X-direction *(b) Y-direction*

Figure 11 - Deformed shapes of the model after pushover analyses

The progression of the important events during the analysis is illustrated on the pushover curve in Figure 12, and it can easily be seen that the structure attains its base shear capacity at about 35 mm structural sway, when the structure nears to an unstable state where the number of failing elements increases unpredictably. Considering these results, *Immediate Occupancy* damage level has been selected as the stage where the first buckling members occur back at the staircase, and not the stage where the first hinge in a stud is observed. This assumption aims at prioritizing the importance of the stairwell rather than just any studs. It may be argued that prioritizing the staircase above all other structural components sounds more like a *life safety* condition. However, it should be noted that the proposed IO damage level only corresponds to the *first* plastic hinge in the staircase, which occurs at a reasonable displacement level of about 2.0 cm. Defining the same displacement as a life safety limit could as well be considered as over-design.

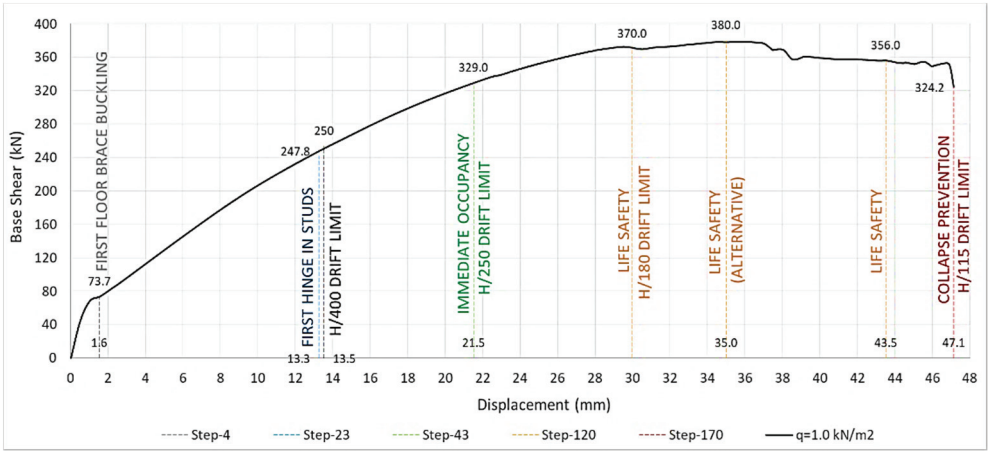

Figure 12 - Significant event progression and the proposed structural damage levels

Life Safety damage level, on the other hand, has been selected as the penultimate stage just before a multiple failure progression starts in any member. Understandably, *Collapse Prevention* damage level has been selected as the final point on the curve. Obviously, LS and CP damage levels appear too close for comfort, thus it is fair to say that LS damage level could as well be taken as the reference point in the design process. It may also be logical to shift LS damage level to the stage where the ultimate base shear is attained, which in this case corresponds to about 30-35 mm structural sway. While it is feasible according to the curve, it should be noted that this displacement level does not appear to physically represent a milestone in the performance history of the building. There are on-going hinge formations in the panels, yet it is difficult to ascertain which of the failing elements at this stage should define the 'life safety' limits.

A structural drift limit of $H/400$, where H is the height of the building, has also been considered. Excluding the rooftop, the effective height of this building is 5.40 m, and thus the allowable drift limit corresponds to 13.5 mm of structural sway. It has been demonstrated that this sway level corresponds to the very first plastic hinge occurring in a stud. In a similar way, it can be said that the proposed IO damage level corresponds to a structural drift limit of $H/250$. Similarly, CP damage level is attained at a structural drift of about $H/115$. Therefore, it can be surmised that LS damage level should bracket these limits, such as $H/180$. This translates to a 30 mm displacement, which in this case roughly corresponds to the stage where the base shear capacity is reached. It is important to note that the use of $H/400$ limit here can be considered as a second method for determining the conventional elastic limit of the pushover curve. It is known that there are two methods available for determining the elastic limit of force-displacement relationships. One of them considers that the initial stiffness can be taken as the secant stiffness to the load level of $0.4\times F_{max}$., as demonstrated and outlined in AISI S213 (25). In the other method proposed by Kawai et al. (26), the initial stiffness is considered as the secant stiffness to the drift level of $H/400$. A detailed interpretation for both methods is provided in the following section.

3.3. Evaluation of the Force Modification Factors

An additional analysis option was examined which also considered post-buckling in the structural elements. A post-buckling strength of 5-10% higher (depending on the section properties) was defined for CFS members, and their respective hinge behavior characteristics were adjusted. This method was attempted to see if the analysis results could be any different. In the end, it was observed that the results yielded only minor discrepancies, as illustrated in Figure 13.

These results must have been expected, because it was shown that the progression of plastic hinges in the studs appeared very late, yet very rapidly. The nonlinear behavior of the structure remained almost indifferent, since the only elements in the structure that would be in their 'post-buckling' state (before any stud reached the buckling load limit) would have been braces. In contrast, their failures appear earlier, and since their load carrying capacity is relatively very low, any post-buckling strength they would acquire would not change the overall nonlinear behavior of the structure. In other words, the post-buckling strength of the braces is very low (due to inherent small capacity) and therefore could be neglected. The post-buckling strength of the studs could also be neglected, since any hinge formation in the studs begin much later, so it does not have a considerable effect on the structural behavior

before the state of collapse. Therefore, the analysis results obtained without post-buckling option were retained.

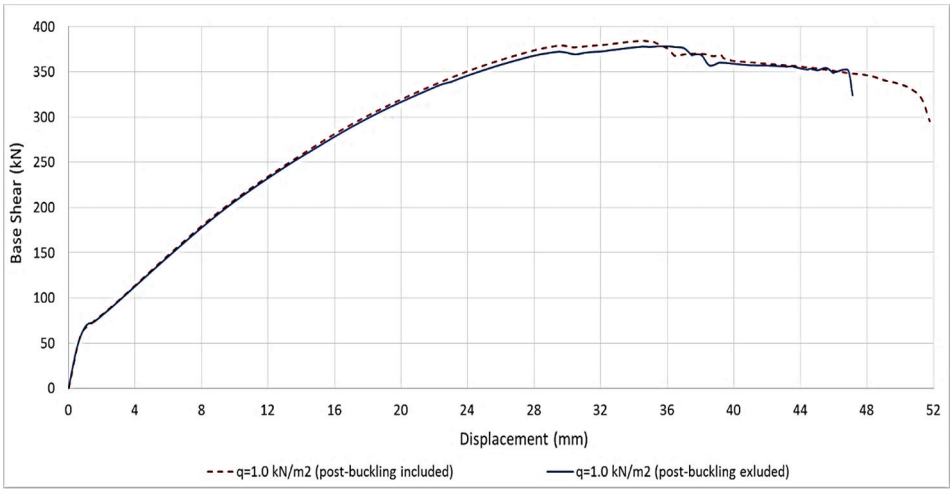

Figure 13 - Pushover analysis results with and without post-buckling effect

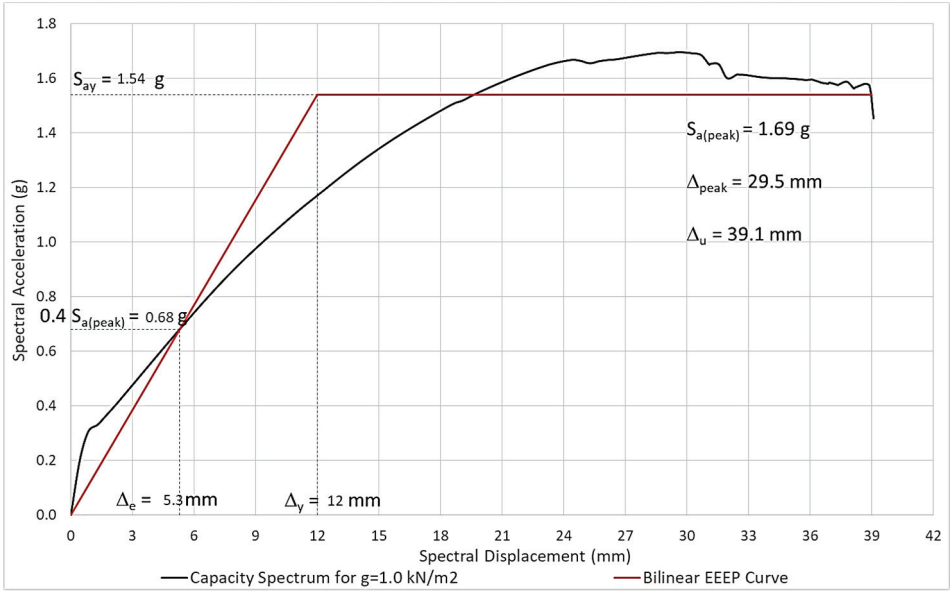

Figure 14 - Performance assessment in Y-direction

Other than that, it may be proper to add a few comments regarding the structural stiffness abruptly decreasing in the initial stages of the analysis. Obviously, this breaking point on the capacity curve does not predominantly represent the general structural behavior. This portion

of the curve may always be approximated to a smoother transition. However, the structure does behave in a linear fashion at the very beginning of the analysis. It should be fair to consider that if all structural elements (links, frames, etc.) could retain their elasticity, the structural response would have remained completely linear, and would follow up on the slope of this very steep initial portion of the curve. Thus, it is concluded that this initial portion must remain as it is in the related figures.

Evaluation of the seismic force modification factors is described in the Appendix 4A of the latest Turkish Seismic Code. Having converted the pushover curves for both X- and Y-directions into ADRS format (Acceleration-Displacement Response Spectra), performance assessment of the building starts with generating a bilinear EEEP (Equivalent Energy Elastic Plastic) approximation of the capacity curve. Figure 14 illustrates the determination of the bilinear EEEP curve for the pushover analysis in Y-direction, which is covered here for the sake of simplicity. The yield displacement is calculated to be Δ_y = 27.7 mm, and the ultimate displacement is Δ_u = 65.2 mm, which denotes the collapse point.

According to the Code, this specific building can be categorized as a structural system with limited ductility, for which the Structural Behavior Factor is defined as R = 3 and the Overstrength Factor is given as D = 2. These values correspond to a ductility ratio of μ_k = 1.5, as given in Equation 1, which is provided by the Code in Appendix 4A.3.1.

$$\frac{R}{I} = \mu_k * D \quad \rightarrow \quad \mu_k = \frac{R}{I*D} = \frac{3}{1*2} = 1.5 \qquad [1]$$

where I is the Importance Factor, which is I = 1. However, the bilinear EEEP curve indicates that the real ductility ratio must be,

$$\mu_k = \frac{\Delta_u}{\Delta_y} = \frac{39.1}{12} = 3.26 \qquad [2]$$

By substituting this value in Equation (1), the Structural Behavior Factor is computed as,

$$R = I * \mu_k * D = 1 * 3.26 * 2 = 6.5 \qquad [3]$$

which is more than twice the value defined in the Code. For comparison, the values of the Force Modification Factors (R_a) computed by using the default values in the Code and by using the ductility ratio obtained from the pushover analysis are given in Equations (4)-(5). It may be concluded from these results that the seismic force reduction factors tend to increase compared to those calculated with the default Code values, i.e. the seismic forces could have been reduced further.

$$R_a = D + \left(\frac{R}{I} - D\right)\frac{T}{T_B} = 2 + (3-2)\frac{0.1}{0.52} = 2.19 \qquad (\textit{TSC 2018}) \qquad [4]$$

$$R_a = D + \left(\frac{R}{I} - D\right)\frac{T}{T_B} = 2 + (6.5-2)\frac{0.1}{0.52} = 2.86 \qquad (\textit{Pushover analysis}) \qquad [5]$$

It is interesting to note that using the drift limit H/400 here for determining the elastic limit is impractical, since the drift value of 13.5 mm corresponds to a spectral displacement of

about 11.0 mm. This value is just too large to be the elastic limit for the capacity curve in Y-direction and using this drift limit can only yield to unreliable calculations.

A brief interpretation of the Overstrength Factor should be made at this point. The value provided in TSC 2018 is intentionally preserved for above calculations since the computation of the factor varies from code to code. In TSC 2018 it is defined as the yield force value obtained from the EEEP approximation by the force value at which the first yielding in the structure takes place. Since there are very slender members such as braces in the structure, it can be claimed that buckling occurs at very early stages, which is testified by the analysis results. However, this may not always be considered as 'yielding', and it may be feasible to investigate for other structural members which undergo higher levels of deformations: positive elongations, for example. Identifying such members may not always be an easy task, and the obtained results may always be debatable, which may lead to unreasonably low or high overstrength values. Hence, the default value provided in the Code is utilized in order to eliminate any disputable results.

There is also another interesting aspect that needs to be pointed out at this stage. An elaborate observation of the hysteresis curves obtained from laboratory experiments (see Figure 7) hints that the envelopes of the curves appear to break slightly at a load level of about $0.3\times F_{max}$. This point may also be considered as the yielding point since a significant decrease in stiffness takes place. However, the same trend does not persist in the force-displacement curves of the building model, apart from the obvious breaking in the initial portion. This may be attributed to the fact that component-based behavior may not always represent the full-scale structural response. In this specific case, for example, taking the $0.3\times P_{peak}$ value as the conventional elastic limit results in a smaller yield displacement, and consecutively a larger ductility ratio, which then only exaggerates the already higher force modification factors. Thus, it can be concluded that the existing assumption of $0.4\times P_{peak}$ for the elastic limit is reasonable.

4. ADDITIONAL ANALYSES WITH VARIABLE PROPERTIES

The variation of R values with regards to changeable design parameters is investigated through additional numerical studies. Again, it should be noted that only the capacity spectra in Y-direction are considered for the sake of simplicity, and that the pushover curves are only plotted up to the point where the analysis results are considered to be reliable.

4.1. Gravity Loading Variations

The results indicate that both base shear and deformation capacity of the structure tend to decrease with higher gravity loads (as expected). It was also observed that the gravity load levels and their distribution along the building influence the capacity spectrum (see Figure 15). Load distribution mainly dominates the first mode shape, resulting in varying capacity spectra with increasing gravity loads. It must be noted that the natural vibration period of the building changes as well. It can be concluded that Structural Behavior Factor varies with respect to the magnitude and distribution of the gravity loads. Performance-wise, it is observed that ductility ratios fluctuate between 3.08 and 3.70, where values generally tend to decrease with higher gravity load levels.

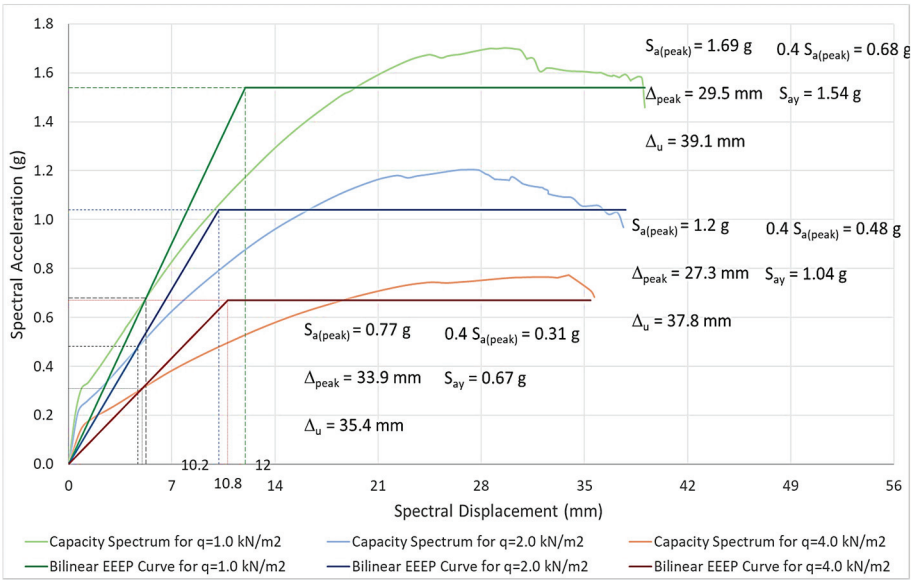

Figure 15 - Performance-based computations for analysis models with varying gravity loads

4.2. OSB Shear Panel Variations

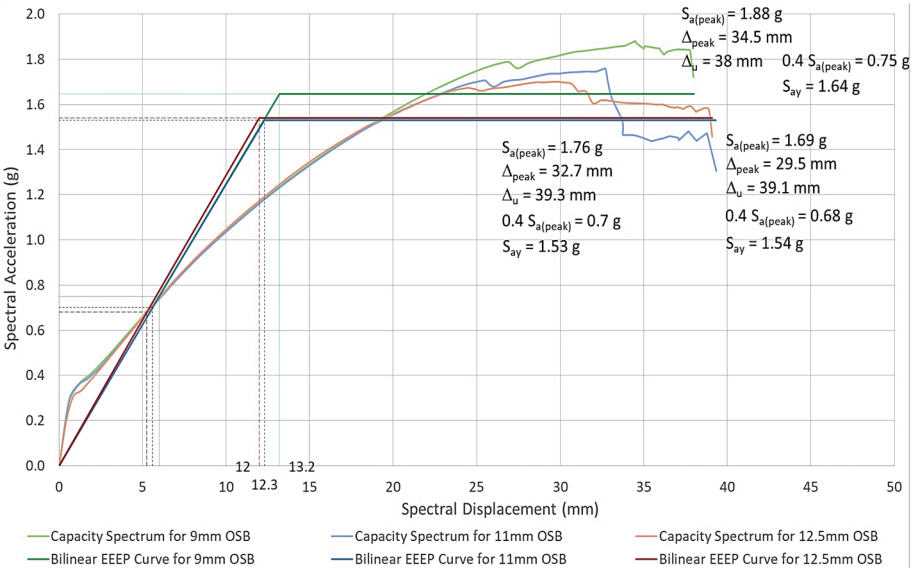

Figure 16 - Performance-based computations for analysis models with varying OSB panel thickness

For this investigation, gravity load levels are taken as 1.0 kN/m^2 live loads in addition to 1.0 kN/m^2 superimposed dead loads. It was observed that the natural vibration period of the

building did not change by much, thus the original value is used in the calculations. It can be concluded from the results (see Figure 16) that both base shear and structural deformation capacities do not vary greatly with respect to panel thickness. Here, it is observed that ductility ratios fluctuate between 2.90 and 3.26, where values tend to increase with panel thickness.

4.3. Gypsum Shear Panel Variations

Similar to the previous investigation, a live load level of 1.0 kN/m^2 in addition to 1.0 kN/m^2 superimposed dead loads is taken as gravity loads. Again, it was observed that the natural vibration period of the building did not change by much, thus the original value is used in the calculations. By looking at the results (see Figure 17), it can be concluded that both base shear and structural deformation capacities do not change by much with respect to panel thickness, in fact they look almost identical. Ductility ratios fluctuate between 6.25 and 7.30, where values tend to increase with respect to panel thickness.

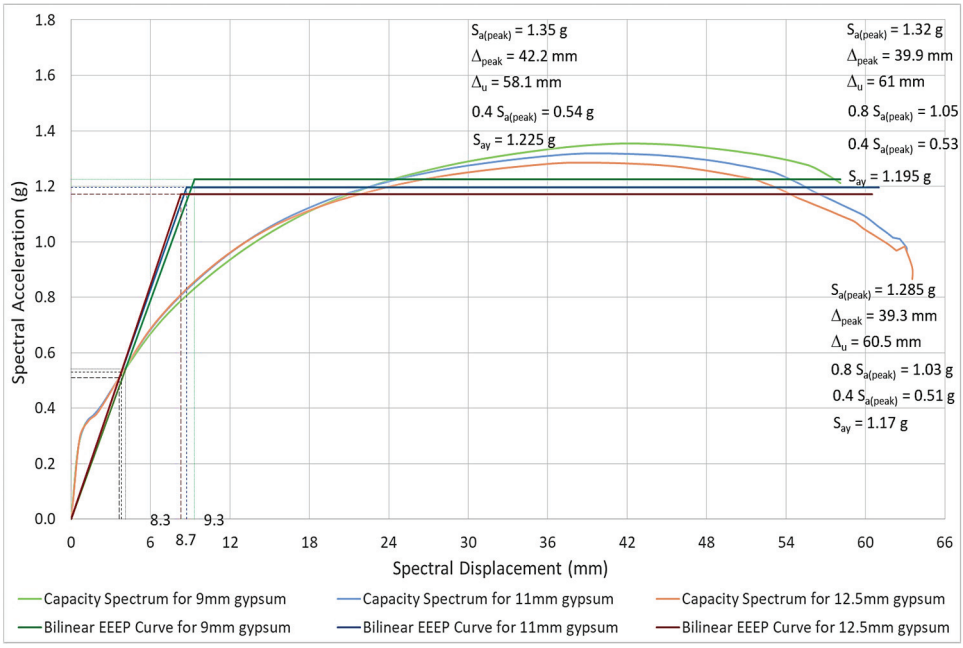

Figure 17 - Performance-based computations for analysis models with varying gypsum panel thickness

4.4. Connection Rigidity Variations

The original screw spacing is kept unaltered for all analyses for the sake of simplicity. Thus, varying levels of robustness is taken into consideration for singular connections. 'Mild connection' corresponds to one-half *F-d* values, and 'stiff connection' means twice as much *F-d* values than those given for the original set of connections.

It can be concluded from the results that using a stiffer connection type increases both the base shear and the structural deformation capacities (see Figure 18). It is also observed that ductility ratios range between 2.55 and 5.00, where values decrease with higher robustness. It should be noted that the applied gravity loads are 1.0 kN/m^2 live loads in addition to 1.0 kN/m^2 superimposed dead loads, and that the natural vibration period of the building does not change by much.

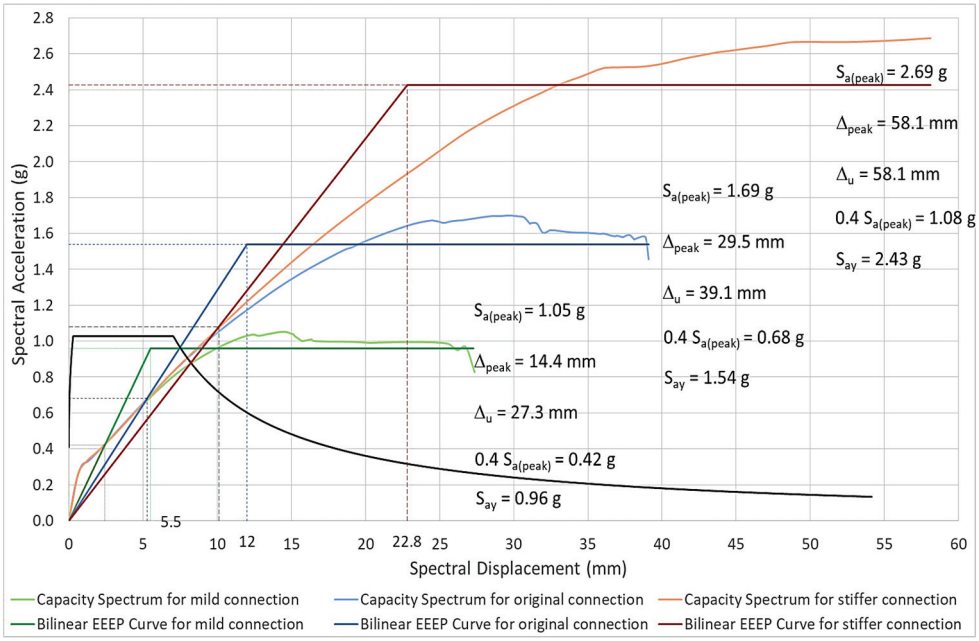

Figure 18 - Performance-based computations for analysis models with varying connection stiffness

5. RESULTS AND OTHER CONSIDERATIONS

It is certain that results obtained from only one building are not sufficient to draw a precise picture. In this specific study, it was shown that the Structural Behavior Factors calculated from the pushover analysis results were generally higher than those defined in TSC 2018. In some cases, calculated values appeared to go up by as much as three times, which is in fact higher than they normally should be. There is always an inevitable possibility of numerical errors in such sensitive analyses, therefore it is essential that these results are backed by further studies. The Structural Behavior Factor definition of the Code may as well be interpreted as having a decent margin for safety. Some other conclusions that can be drawn from this study are outlined below.

1. Both base shear capacity and deformation capacity of the structure tend to decrease with higher gravity loads. Also, the applied gravity loads and their distribution along the building greatly effects the structural capacity spectrum. Load distribution mainly dominates the first mode shape, i.e. the natural vibration period(s) of the building changes

with increasing load levels. In conclusion, Structural Behavior Factor varies with respect to the magnitude and distribution of the gravity loads.

Although not perfectly fit, the proposed approximate trend-line (see Figure 19) suggests that the ductility ratio (hence the Structural Behavior Factor) should decrease with increasing amount of dead and live loads, which sounds meaningful to some degree. The notation 'seismic weight ratio' in the figure corresponds to the total seismic weight computed in compliance with the Code, divided by the dead weight of the building, rooftop and sidewall claddings included. For example, the self-weight of the building is 165 kN according to analysis results, while the seismic weight of the building is calculated as 267.1 kN for the gravity loading case where dead loads are 1.0 kN/m^2 and live loads are 1.0 kN/m^2. This gives the ratio of 1.62, which is the lowest value on the figure. For higher levels of the gravity loading, higher seismic weight ratios are obtained, which are subsequently indicated on the figure. When there are absolutely no loads acting on the structure, i.e. the very initial case where the structure has just been constructed, the seismic weight ratio of the structure is 1.0, according to the above definition. In this case, trend-line suggests that the ductility ratio could be just about 3.5.

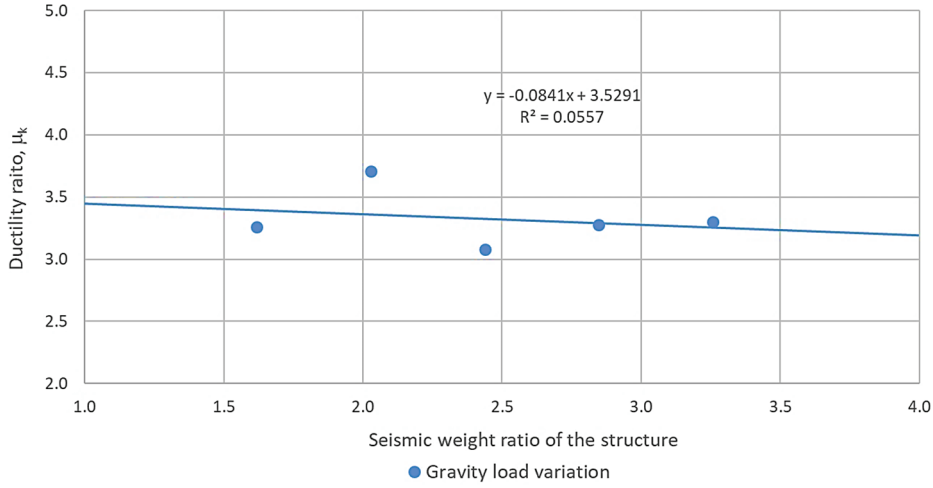

Figure 19 - The variation of the ductility ratio with respect to varying gravity load levels

2. For a predefined level of the gravity loads, OSB or gypsum thickness is nearly ineffectual on either the resultant base shear capacity or the resultant structural deformation capacity. The calculated values of the ductility ratio for both panel types are illustrated in Figure 20, along with their trend-lines. It should be noted that the Structural Behavior Factors are simply twice their respective ductility values, according to the assumptions $D = 2$ and $I = 1$.

It is evident that the ductility appears to be higher in buildings with gypsum-sheathed CFS shear walls. Also, the variation of the ductility ratio with respect to panel thickness is greater with gypsum panels. The proposed trend-lines suggest that, while an average

value could be applied for the Structural Behavior Factor in buildings with OSB-sheathed CFS shear walls, *R* values should be increased along with greater values of board thickness in buildings with gypsum-sheathed CFS shear walls. It is fair to say that TSC 2018 lacks necessary guidelines in this aspect and should be modified.

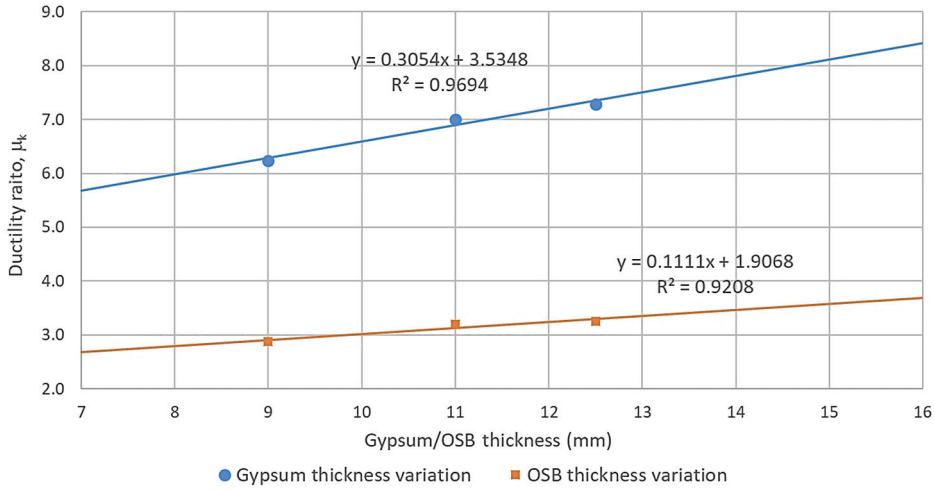

Figure 20 - The variation of the ductility ratio with respect to gypsum & OSB thickness

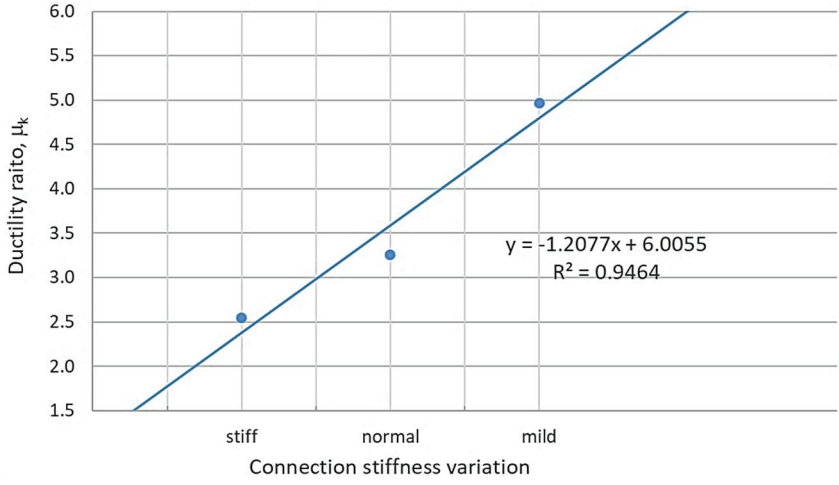

Figure 21 - The variation of the ductility ratio with respect to connection stiffness

3. Regarding the rigidity level of a single frame-to-frame or frame-to-panel connection, it was shown that using a stiffer connection type greatly increases both the base shear capacity and the structural deformation capacity. However, the proposed trend-line (see Figure 21) suggests that the stiffer they are, the smaller is the Structural Behavior Factor.

While this is somewhat addressed in TSC 2018 by defining a lower *R* value for structural systems with limited ductility, there is no exact definition of a structural system with limited ductility, other than the referral to utilizing braces and/or gypsum panels within the structure. There is no example of what ductility level should be considered for buildings where OSB panels *and* braces are used together, for example. In this specific study, it was shown that in such systems the ductility ratio could be as much as 5.0 or even greater.

6. CONCLUSIONS

Although this construction material can be regarded as one of the most reliable, it may still contain imperfections. Moreover, a cold-formed steel section is arguably more sensitive to faulty workmanship during the construction phase: even the slightest tilting or bending of the member may cause significant second-order stress concentrations within the cross-section. Thus, it may be helpful to introduce a safety factor (γ_m) as caution. Taking this into account, the formulations given in Chapter 5 can be rewritten as below.

for considering the effect of gravity loading:

$$R = \frac{I*D}{\gamma_m}\left(3.5 - \frac{W_E}{12W}\right) \quad [6]$$

(where W_E is the total seismic weight, and W is the dead weight of the structure)

for OSB-sheathed CFS buildings with double-X strap braces:

$$R = \frac{I*D}{\gamma_m}\left(\frac{t}{9} + 1.9\right) \quad \text{(where t is panel thickness)} \quad [7]$$

for gypsum-sheathed CFS buildings with double-X strap braces:

$$R = \frac{I*D}{\gamma_m}\left(\frac{t}{3.3} + 3.5\right) \quad \text{(where } t \text{ is panel thickness)} \quad [8]$$

While it is obvious that stiffer connections are less ductile, it is difficult to formulate this relationship. As already stated, many factors contribute to the connection rigidity, and should be separately analyzed. Here for this case study, only the screw cross-section is considered for the sake of simplicity. Thus, an equation can be formulated as in Eq. (9).

$$R = \frac{I*D}{\gamma_m}\left(6 - \frac{1.2A}{A_{ref}}\right) \quad [9]$$

where A is the area of the screw cross-section, and A_{ref} is a reference screw section. Instead of area proportioning, the term d/d_{ref} may also be preferred since the diameter of the screw can be more of a meaningful criterion in design. Here it is important to determine a reference screw section (d_{ref} or A_{ref}), and a benchmark experiment may be required to define a standard ductility level. The screws used in this experiment may be accepted as A_{ref} or d_{ref} for example,

and the effect of different screw sections on the structural behavior factor can be put into numbers with the above formula.

It was shown in this specific example that the ductility ratio, hence the Structural Behavior Factor generally decreases with increasing gravity loads. The reason for this was based on the load distribution within the building, thus affecting the structural mode shapes. Load distributions may not always be similar in different types of buildings. However, if additional studies on the same subject support this trend, i.e. R values decrease with gravity loads, it may be convenient to associate the values in the Code with the design loads of a structure. In practice, this could mean that the Structural Behavior Factors of a CFS-framed residential building and a CFS-framed school or hospital, for instance, would not be the same.

It is also worthwhile to recall for the sake of simplicity that, the analytical the analytical studies within this study only included the investigation of the structural performance with respect to the rigidity of a singular connection,. The rigidity of a single connection may as well originate from the thickness of the screws, the thickness of the frame cross-section, the thickness of the panels, or a combination of all of these. It was shown that the increasing connection stiffness yields a higher base shear capacity and a higher deformational capacity. Yet, the exact manner by which the connection stiffness is doubled or tripled is open to discussion. Thus, it may also be interesting to see if structural performance is anyhow affected by varying screw spacing, which is a more meaningful interpretation of connection rigidity.

Symbols

A	Area of the screws
A_{ref}	Area of a reference set of screws
d	Displacement (or deformation); screw diameter
d_{ref}	Diameter of a reference set of screws
D	Overstrength factor, as defined in TSC 2018
F	Force
F_{max}	Peak value of the force
g	Gravitational acceleration; gravity loads (superimposed dead loads)
H	Height of the structure
I	Earthquake importance factor of the structure
P_{peak}	The peak value of base shear (or force)
q	Live loads
R	Response modification factor; structural behavior factor
R^2	Proportion of variance
R_a	Seismic force reduction factor

$S_{a(peak)}$	The peak value of spectral (response) acceleration
S_{ay}	Spectral (response) acceleration at yield
t	Panel thickness
T	Period; the fundamental period of the building
T_B	Upper corner period of the elastic design acceleration spectrum
T_i	The natural vibration period related to the i^{th} structural mode
W	Dead weight of the structure
W_E	Total seismic weight (computed in accordance with TSC 2018)
Δ_e	Elastic displacement
Δ_{peak}	The displacement value at peak response acceleration level
Δ_u	Ultimate displacement
Δ_y	Yield displacement
γ_m	Factor of safety
μ_k	Ductility ratio

Acknowledgements

The authors acknowledge the Department of Civil Engineering of Boğaziçi University for the technical support to the research activity, and Akkon Celik Yapi Sistemleri A.Ş. for the procurement of the steel strap-braces for laboratory experiments, and the real-life building for ambient vibration tests. The authors would also like to thank the anonymous reviewer for the precious comments and suggestions to improve the quality of the paper.

References

[1] Türkiye Bina Deprem Yönetmeliği, Deprem Etkisi Altında Binaların Tasarımı İçin Esaslar, T.C. İçişleri Bakanlığı Afet ve Acil Durum Yönetimi Başkanlığı, Ankara, Türkiye, 2018.

[2] Della Corte, G., Fiorino, L., Landolfo, R., "Seismic behavior of sheathed cold-formed structures: numerical study", *Journal of Structural Engineering*, 132(4), 558-569, 2006.

[3] Landolfo, R., Fiorino, L., Della Corte, G., "Seismic behavior of sheathed cold-formed structures: physical tests", *Journal of Structural Engineering*, 132(4), 570-581, 2006.

[4] Dubina, D., "Behavior and performance of cold-formed steel-framed houses under seismic action", *Journal of Constructional Steel Research*, 64, 896-913, 2008.

[5] Velchev, K., Comeau, G., Balh, N., Rogers, C.A., "Evaluation of the AISI S213 seismic design procedures through testing of strap braced cold-formed steel walls", *Thin-Walled Structures*, 48, 846-856, 2010.

[6] Nithyadharan, M., Kalyanaraman, V., "Behavior of cold-formed steel shear wall panels under monotonic and reversed cyclic loading", *Thin-Walled Structures*, 60, 12-23, 2012.

[7] Shamim, I., Rogers, C.A., "Steel sheathed/CFS framed shear walls under dynamic loading: numerical modelling and calibration", *Thin-Walled Structures*, 71, 57-71, 2013.

[8] Sato, A., Uang, C.M., "A FEMA P695 study for the proposed seismic performance factors for cold-formed steel special bolted moment frames", *Earthquake Spectra*, 29(1), 259-282, 2013.

[9] Iuorio, O., Macillo, V., Terracciano, M.T., Pali, T., Fiorino, L., Landolfo, R., "Seismic response of CFS strap-braced stud walls: experimental investigation", *Thin-Walled Structures*, 85, 466-480, 2014.

[10] Bian, G., Padilla-Llano, D.A., Buonopane, S.G., Moen, C.D., Schafer, B.W., "OpenSees modeling of a wood-sheathed cold-formed steel-framed shear walls", *Proceedings of the Annual Stability Conference*, Structural Stability Research Council, Nashville, Tennessee, March, 2015.

[11] Senkardesler, O., Goler, G., Soyoz, S., "Dynamic and cyclic response of a full-scale 2-story cold-formed steel structure with and without infill materials", *Bulletin of Earthquake Engineering*, 15(8), 3207-3326, 2016.

[12] Borzoo, S., Mir Ghaderi, S.R., Mohebi, S., Rahimzadeh, A., "Nonlinear finite element modeling of steel-sheathed cold-formed steel shear walls", *Steel and Composite Structures*, 22(1), 79-89, 2016.

[13] Madsen, R.L., Castle, T.A., Schafer, B.W., "Seismic design of cold-formed steel lateral load-resisting systems: a guide for practicing engineers", *NEHRP Seismic Design Technical Brief No.12*, Engineering Laboratory, National Institute of Standards and Technology, Gaithersburg, Maryland, August, 2016.

[14] Karabulut, B., Soyoz, S., "Experimental and Analytical Studies on Different Configurations of Cold-Formed Steel Structures", *Journal of Constructional Steel Research*, 133, 535-546, 2017.

[15] Leng, J., Peterman, K.D., Bian, G., Buonopane, S.G., Schafer, B.W., "Modeling seismic response of a full-scale cold-formed steel-framed building", *Engineering Structures*, 153, 146-165, 2017.

[16] Riahi, H.T., Zeynalian, M., Rabiei, A., Ferdosi, E., "Seismic collapse assessment of K-shaped bracings in cold-formed steel frames", *Structures*, 25, 256-267, 2020.

[17] Haghpanah, F., Schafer, B.W., "Updated seismic fragility functions for cold-formed steel framed shear walls per FEMA P-58 methodology", *Engineering Structures*, 244:112753, 2021.

[18] Yurtsever, M., "Ortamsal titreşim deneyleriyle hafif-çelik yapılarda titreşim periyotlarının belirlenmesi ve doğrulanması", *Çelik Yapılar*, 55, 38-45, 2018.

[19] CSI SAP2000 v20.2.0, *Integrated Finite Element Analysis and Design of Structures*, Computers and Structures Incorporated, Berkeley, California, 2019.

[20] Yurtsever, M., "An investigation on force modification factors in cold-formed steel structures", Ph.D. Dissertation, Boğaziçi University, Istanbul.

[21] ASTM E2126, *Standard Test Methods for Cyclic (Reversed) Load Test for Shear Resistance of Vertical Elements of the Lateral Force Resisting Systems for Buildings*, American Society for Testing and Materials International, West Conshohocken, Pennsylvania, USA, 2011.

[22] GBTUL 2.06, *Generalized Beam Theory at the University of Lisbon*, Generalised Beam Theory Research Group, Instituto Superior Técnico, University of Lisbon, 2016.

[23] CUFSM 5.01, *Constrained and Unconstrained Finite Strip Method*, Thin-Walled Structures Group, Department of Civil and Systems Engineering, Johns Hopkins University, Baltimore, 2019.

[24] CUTWP, *Cornell University Thin-Walled (Section) Properties*, Cold-Formed Steel Structures Research Group, School of Civil and Environmental Engineering, Cornell University, Ithaca, New York, 2003.

[25] AISI S213-07 w/S1-09, *North American Standard for Cold-Formed Steel Framing – Lateral Design*, American Iron and Steel Institute, Washington D.C., USA, 2012.

[26] Kawai Y., Kanno R., and Hanya K., "Cyclic shear resistance of light-gauge steel framed walls", *ASCE Structures Congress*, Poland, USA, 433-437, 1997.